Evolution of Shear Fabric in Granular Fault Gouge From Stable Sliding to Stick-Slip and Implications for Fault Slip Mode

M.M. Scuderi[1], C. Collettini[1], C. Viti[2], E. Tinti[3] and C. Marone[4]

[1] *Dipartimento di Scienze della Terra, La Sapienza Università di Roma, Rome Italy*

[2] *Dipartimento di Scienze Fisiche, della Terra e dell'Ambiente, Università degli Studi di Siena, Siena, Italy*

[3] *Istituto Nazionale di Geofisica e Vulcanologia (INGV), Rome Italy*

[4] *Department of Geoscience, The Pennsylvania State University, University Park, PA USA*

*Correspondence to: marco.scuderi@uniroma1.it

ABSTRACT

Laboratory and theoretical studies provide insight into the mechanisms that control earthquake nucleation, when fault slip velocity is slow (<0.001 cm/s), and dynamic rupture when fault slip rates exceed cm/s. The application of these results to tectonic faults requires information about fabric evolution with shear and its affect on the mode of faulting. Here we report on laboratory experiments that illuminate the evolution of shear fabric and its role in controlling the transition from stable sliding (v~0.001 cm/s) to dynamic stick-slip (v>1 cm/s). The full range of fault slip modes was achieved by controlling the ratio, $K = k/k_c$, where k is the elastic loading stiffness, and k_c is the fault zone critical rheologic stiffness. We show that K controls the transition from slow-and-silent slip ($K > 0.9$) to fast-and-audible ($K < 0.7$, v = 3 cm/s, slip duration 0.003 s) slip events. Microstructural observations show that with accumulated strain, deformation concentrates in shear zones containing sharp shear planes made of nano-scale grains, which favour the development of frictional instabilities. Once this fabric is established, fault fabric does not change significantly with slip velocity, and fault slip behaviour is mainly controlled by the interplay between the rheological properties of the slipping planes and fault zone stiffness. As applied to tectonic faults, our results suggest that a single fault segment can experience a spectrum of fault slip behaviour depending on the evolution of fault rock frictional properties and viscoelastic properties of the wall rock surrounding the fault.

INTRODUCTION

Understanding the relationship between the evolution of fault fabric and fault slip behaviour is a long-standing problem in fault mechanics. Tchalenko (1970) used shear box experiments to document fault zone evolution, from Riedel shears to boundary parallel shears with increasing strain. The similarities of the experimental fault zone structure with earthquake faulting were interpreted as indicating similarities in the deformation mechanism (Tchalenko, 1970). Several laboratory and field studies have expanded on the kinematic descriptions, with the aim of developing an integrated understanding of the evolution of fault zone microstructure and friction constitutive properties (e.g. Sibson, 1977; Logan et al, 1979; Yund, 1990; Marone and Kilgore, 1993; Beeler et al., 1996). For quartzo-feldspatic fault gouge, increasing strain causes an evolution from distributed to localized deformation along fault parallel shear planes. This microstructural evolution is accompanied by a transition from a velocity strengthening (i.e. aseismic creep) to velocity weakening behavior, which is a necessary condition for frictional instability (e.g. Marone, 1998).

In the last decade, high-velocity friction experiments have shown that at earthquake slip velocities (≥10cm/s) significant grain-size reduction and localization occurs in granular materials (e.g. Goldsby and Tullis 2002; Hirose and Shimamoto, 2005; Reches and Lockner 2010; Di Toro et al., 2011; De Paola et al., 2015; Smith et al., 2015). These studies have been fundamental to characterize fault rocks produced during the earthquake slip phase, however, these experiments are conducted with imposed co-seismic velocities, whereas along natural faults the instability arises spontaneously and is driven by the elastic interaction between the fault zone and the surrounding (e.g. Scholz, 2002). Stick-slip frictional sliding experiments have provided the foundation for earthquake physics (e.g. Brace and Byerlee, 1966; Scholz et al., 1972, Okubo and Dieterich, 1984). Recently, stick-slip experiments on bare rock surfaces have documented the melting of asperity contacts of the slipping surface during large stress drops (e.g. Brantut et al., 2016; Hayward et al., 2016; Passelègue et al., 2016). Despite these significant scientific advancements on the mechanics

of stick-slips along bare rock surfaces, the mechanisms for strain localization and fault weakening during stick-slip frictional instabilities within fault gouge are still poorly understood. In this manuscript we build on recent works that documented the spectrum of fault slip behaviour, from stable sliding to stick-slip on quartz gouge (Leeman et al., 2016; Scuderi et al., 2016; Tinti et al., 2016), to characterize the evolution of shear fabric from stable sliding to stick-slip and infer the controlling mechanism for different fault slip behavior.

METHODS

Frictional stick-slip instabilities occur when the fault-weakening rate with slip exceeds the maximum rate of elastic unloading, resulting in a force imbalance and acceleration (e.g. Scholz, 2002). In the simplified case of an experimental fault obeying rate- and state-friction (RSF) laws the possibility to develop stick-slip instabilities is controlled by the interaction between the system elastic stiffness, k, and the fault frictional properties, which can be written in terms of a critical rheologic stiffness k_c (Gu et al., 1984). The condition for the nucleation of instability, when sliding velocity is still slow, is:

$$k < k_c = \frac{\sigma`_n(b-a)}{D_c} \qquad (1)$$

where $\sigma`_n$ is the effective normal stress, *(b-a)* is the friction rate parameter and D_c is the critical slip distance. The ratio $K=k/k_c$ describes fault stability: under quasi-static conditions, where accelerations are negligible, sliding is stable for $K>1$ and unstable for $K<1$.

To explore the relationship between shear fabric evolution and the mode of fault slip, we conducted laboratory experiments using the double-direct shear configuration in a biaxial deformation apparatus (Fig. 1A) (Collettini et al., 2014). Fault zones were composed of quartz gouge (99.5% SiO_2), with a grain-size in the range of 2-50 μm and mean size of 10-15 μm. Gouge

layers were sheared at constant velocity of 10 μm/s and normal stresses ranging from 13 to 35 MPa (Table DR1 in the GSA Data repository). We performed velocity step experiments to retrieve the RSF parameters and characterize the fault critical rheologic stiffness, k_c (Fig. DR2 in the GSA Data Repository). To explore a range of stability conditions at different values of K, we artificially reduced our shear loading stiffness by inserting an elastic element in the loading column (Fig. 1A). For these conditions, the transition from stable to unstable sliding occurs at 14 MPa (Fig. 1B), and we explored a range of normal stresses up to 35 MPa to study the transition from stable to unstable sliding (Fig. 1B and C). At the end of the experiments we collected samples for Scanning Electron Microscopy, SEM, and Transmission Electron Microscopy, TEM, investigations. We also analyzed microstructures for experiments at low and high shear strain that were performed at higher stiffness, resulting in stable sliding at normal stress of 25 MPa.

COUPLING BETWEEN MECHANICAL AND MICROSTRUCTURAL EVOLUTION

Our experiments document a spectrum of slip behaviours from stable to quasi-dynamic and fully dynamic sliding (Fig. 1B and C). With decreasing K the recurrence time of stick-slip cycles becomes longer, the stress drop increases from ~ 0.4 to ~ 2.4 MPa and the slip velocity increases from ~ 150 μm/s for K = 0.9 to ~ 3 cm/s for K = 0.5 (Fig. 1C).

We document a systematic evolution of the microstructure with strain and fault slip behaviour (Fig. 2). At low strain, when shear is stable, microstructural images show angular, unfractured grains with a grain-size comparable to the starting material (Fig. 2A). Some grain-size reduction is evident within proto B-shear zones that are up to 200 μm wide. With increasing strain (Fig. 2B) the B-shear zones become more continuous and contain sub-parallel discrete slip surfaces, Y-shears, where the grain-size reduces to about 1 μm. From low to high strain (Fig. 2C) we document an evolution of *(a-b)* from velocity strengthening to velocity weakening and a reduction of D_c, from 15 to 1 μm, consistent with previous work (Marone and Kilgore, 1993). These changes result in an increase in the critical weakening rate, k_c, for shear strains up to ~5. For $\gamma > 8$, k_c,

reaches a steady value that does not vary appreciably with greater shear (Fig. 2C), indicating that the fault zone has achieved a nearly stable microstructural and mechanical state. We also document a reduction of layer dilation upon velocity steps with increasing strain, which is a further indication of shear localization (Figs. 2D and DR3 in the GSA data repository).

Comparing the fault zone fabric observed during stable sliding at high strain with the microstructure developed after both slow-slip and fast stick-slip we do not observe significant differences (Fig. DR4 in the GSA Data Repository). In both cases, most of the deformation occurs along B-shear zones and it is localized along Y-shears (Fig. 2E). The Y-shears consist of tightly packed portions of randomly-oriented quartz nanograins, with grain dimensions of 50 to 500 nm, characterized by rounded shape and intense dislocations (Fig. 2E green inset). In some instances, grains with dimensions of 0.5 to 1 μm are fractured and show sharp grain-boundaries. Some amorphous material is present at the boundaries of the smaller grains, however the development of amorphous material in high-strain zones is not a prominent feature of the microstructure. Nano-grains, <200 nm, likely form by dislocation pile-up within larger grains. Outside the B-shear zones the quartz grains are larger and contain pervasive fractures (Fig. 2E red inset).

DISCUSSION

Our experiments show that fault slip behaviour is controlled by the interplay between the effective shear loading stiffness ($k' = k/\sigma'_n$) and the effective fault rheological stiffness ($k'_c = (b-a)/D_c$) and their evolution with stress, strain and fabric development (Figs. 3 and DR5 in GSA Data Repository). The stiffness k' varies with fault porosity and particle contact stiffness, which are influenced by fault normal stress and shear enhanced compaction, increasing at low strains before reaching steady state values for $\gamma > \sim 3$. The fault zone rheologic stiffness, k'_c, grows from negative to positive values at low strains, as *(a-b)* transitions from velocity strengthening to velocity weakening (Fig. 2C), and then it increases slowly at higher strain. The evolution of k'_c with increasing strain is further compounded by reduction of D_c, from 15 μm, the average initial grain-

size of the tested material, to sub-micrometric values, which corresponds to the grain size within Y-shears (Fig. 2E).

Our results illustrate how fabric development influences fault slip behaviour and the spectrum of slip modes. At low strain (Fig. 3) shear deformation is distributed and is mainly accommodated by grain rotation, translation and fracturing. Limited grain-size reduction occurs along proto B shear zones and R_1 shears, resulting in large values of D_c and velocity strengthening behaviour. With increasing strain, the B shear zones become more continuous and further localization forms Y-shears, causing smaller values of D_c (Marone and Kilgore, 1993). Shear localization is also documented by a reduction of layer dilation with strain (Figure 2D), which is associated with the transition from velocity strengthening to velocity weakening behaviour (e.g. Beeler et al., 1996; Marone, 1998; Ikari, 2015). At this point, the experimental fault has the necessary condition for instability (a-b < 0). The sufficient condition for instability, which dictates the mode of fault slip, is determined by the stiffness ratio $K = k/k_c = k'/k'_c$ (Fig. 1 and 3). Small stick-slip instabilities initiate spontaneously when K = 1, i.e. near the intersection between the black and red curves shown in Fig. 3. With further shear, as K decreases, stress drop and peak slip velocity increase until a nearly steady state for a given K, with stick-slip behaviour characterized by slow, quasi-dynamic slip or fast, dynamic slip (Fig. 1C and DR6 in the GSA Data Repository). We relate this transition to the growth and interconnectivity of the Y-shears within the B shear zone. After the initial growing phase, stick-slips evolution is controlled by K. Slow earthquakes with slip velocity of ~100 μm/s, stress drop of 0.5 MPa and slip duration of 0.5 s occur for $k'_c \approx k'$ (Fig. 3), and faster events with slip velocity up to 3 cm/s, stress drop 2.4 MPa, slip duration 0.003 are observed when $k'_c > k'$ (Fig. 3).

Our results show that fault zone microstructure is approximately independent of the mode of faulting. The similarities in microstructures, in particular localization along Y-shears, for experimental faults that experienced different slip velocities, ranging from 0.001 to 3 cm/s, indicate that at the tested boundary conditions, once localization is well established, the slip behaviour is

mainly controlled by the stiffness ratio K. Under these conditions, minor changes in frictional rheology, k_c, and/or elastic stiffness of the surrounding result in dramatic changes in the mode of fault slip. For instance, in an experiment started at normal stress of 35 MPa, after recording a series of dynamic stick-slips, we reduced the normal stress to 15 MPa and observed stick-slips with larger stress drop (1 MPa vs. 0.5 MPa) and faster slip velocities (1.5 mm/s vs. 0.15 mm/s) in comparison to standard experiments that started at 15 MPa normal stress (Figure DR7 in the GSA Data Repository). The different fault slip mode, for the same applied normal stress, results from the inherited fault zone stiffness. That is, the elastic stiffness acquired at 35 MPa is maintained when we reduce the stress at 15 MPa dictating the fault slip behaviour. For our standard loading history, fault zones sheared at 15 MPa normal stress have lower stiffness than those at 35 MPa, produced by lesser grain-size reduction and greater porosity (Fig. DR6 in the GSA Data Repository). These data indicate that structural and microstructural evolution of the loading medium surrounding the area of slip localization can significantly influence fault slip behaviour and the mode of faulting.

As applied to tectonic faults our results suggest that a single fault segment can experience a spectrum of fault slip behaviour depending on the evolution of fault rock frictional properties and elastic conditions of the loading system. This mechanical prediction is consistent with the observation that some slow and fast earthquakes occur on the same fault (e.g. Kato et al., 2012; Ruiz et al., 2014; Veedu and Barbot, 2016). In addition, the stiffness ratio K represents a general mechanism for fault slip behaviour because it includes all the key-parameters that have been used to model the spectrum of fault slip behaviour such as, fluid pressure (e.g. Kodaira et al., 2004; Segall et al 2010), the evolution of frictional properties with fault maturity and depth (e.g. Liu and Rice, 2007; Ampuero and Rubin, 2008) and other viscous processes (e.g. Fagereng et al., 2014; Hayman and Lavier, 2014) that likely influence the effective normal stress and can alter the stiffness of the loading system.

ACKNOWLEDGMENTS

We thank P. Scarlato for support at the INGV HP-HT laboratory. This research was supported by ERC grant Nr.259256 GLASS to CC, NSF-EAR1520760 and DE-EE0006762 to CM, and EU Horizon 2020 Marie Sklodowska-Curie No.656676 FEAT to MMS.

REFERENCES

Ampuero, J.-P., and A. M. Rubin (2008), Earthquake nucleation on rate and state faults – Aging and slip laws, *J. Geophys. Res.*, *113*,doi:10.1029/2007JB005082.

Beeler, N., and T. Tullis (1996), Frictional behavior of large displacement experimental faults, *J. Geophys. Res.*, *101*, 8697–8715.

Brace, W., and J. Byerlee (1966), Stick-Slip as a Mechanism for Earthquakes, *Science*, *153*, 990–992.

Brantut, N., F. X. Passelègue, D. Deldicque, J.-N. Rouzaud, and A. Schubnel (2016), Dynamic weakening and amorphization in serpentinite during laboratory earthquakes, *Geology*, doi:10.1130/G37932.1.

Collettini, C., G. Di Stefano, B. Carpenter, P. Scarlato, T. Tesei, S. Mollo, F. Trippetta, C. Marone, G. Romeo, and L. Chiaraluce (2014), A novel and versatile apparatus for brittle rock deformation, *Int. J. Rock Mech. Min. Sci.*, *66,* doi: 10.1016/j.ijrmms.2013.12.005.

De Paola, N., R. E. Holdsworth, C. Viti, C. Collettini, and R. Bullock (2015), Can grain size sensitive flow lubricate faults during the initial stages of earthquake propagation?, *Earth Planet. Sci. Lett.*, *431*, doi:10.1016/j.epsl.2015.09.002.

Di Toro, G., R. Han, T. Hirose, N. De Paola, S. Nielsen, K. Mizoguchi, F. Ferri, M. Cocco, and T. Shimamoto (2011), Fault lubrication during earthquakes., *Nature*, *471*, doi:10.1038/nature09838.

Logan, J. M., M. Friedman, N. Higgs, C. Dengo, and T. Shimamodo (1979), Experimental studies of simulated fault gouges and their application to studies of natural fault zones, in Analysis of Actual Fault Zones in Bedrock, US Geol. Surv., 1239, 305-343.

Fagereng, Å., G. W. B. Hillary, and J. F. a Diener (2014), Brittle-viscous deformation , slow slip , and tremor, *Geophys. Res. Lett.*, *41*, doi:10.1002/2014GL060433.1.

Goldsby, D. L., and T. E. Tullis (2002), Low frictional strength of quartz rocks at subseismic slip rates, *Geophys. Res. Lett.*, *29*, doi:10.1029/2002GL015240.

Gu, J., J. Rice, A. Ruina, and S. Tse (1984), Slip motion and stability of a single degree of freedom elastic system with rate and state dependent friction, *J. Mech. Phys.*, *32*, 167–196.

Hayman, N. W., and L. L. Lavier (2014), The geologic record of deep episodic tremor and slip, *Geology*, *42*, doi:10.1130/G34990.1.

Hayward, K. S., S. F. Cox, J. D. Fitz Gerald, B. J. J. Slagmolen, D. A. Shaddock, P. W. F. Forsyth, M. L. Salmon, and R. P. Hawkins (2016), Mechanical amorphization, flash heating, and frictional melting: Dramatic changes to fault surfaces during the first millisecond of earthquake slip, *Geology*, doi:10.1130/G38242.1.

Hirose, T., and T. Shimamoto (2005), Growth of molten zone as a mechanism of slip weakening of simulated faults in gabbro during frictional melting, *J. Geophys. Res. Solid Earth*, *110*, doi:10.1029/2004JB003207.

Kodaira, S., T. Iidaka, A. Kato, J.-O. Park, T. Iwasaki, and Y. Kaneda (2004), High pore fluid pressure may cause silent slip in the Nankai Trough., *Science*, *304*, doi:10.1126/science.1096535.

Ikari, M. (2015), Principal slip zones: Precursors but not recorders of earthquake slip, *Geology*, doi:10.1130/G37028.1.

248 Leeman, J. R., D. M. Saffer, M. M. Scuderi, and C. Marone (2016), Laboratory observations of slow earthquakes and
249 the spectrum of tectonic fault slip modes, *Nat. Commun.*, *7*, doi:10.1038/ncomms11104.

250 Liu, Y., and J. R. Rice (2007), Spontaneous and triggered aseismic deformation transients in a subduction fault model,
251 *J. Geophys. Res. Solid Earth*, *112,* doi:10.1029/2007JB004930.

252 Marone, C., and B. Kilgore (1993), Scaling of the critical slip distance for seismic faulting with shear strain in fault
253 zones, *Nature*, *362*, 618–621.

254 Marone, C. (1998), Laboratory-Derived Friction Laws and Their Application To Seismic Faulting, *Annu. Rev. Earth*
255 *Planet. Sci.*, *26*, doi:10.1146/annurev.earth.26.1.643.

256 Okubo, P., and J. Dieterich (1984), Effects of Physical Fault Properties on Frictional Instabilities Produced on simulated
257 Faults, *J. Geophys. Res*, *89*, 5817–5827.

258 Passelègue, F. X., A. Schubnel, S. Nielsen, H. S. Bhat, D. Deldicque, and R. Madariaga (2016), Dynamic rupture
259 processes inferred from laboratory micro-earthquakes, *J. Geophys. Res. Solid Earth*, 121,
260 doi:10.1002/2015JB012694.

261 Reches, Z., and D. A. Lockner (2010), Fault weakening and earthquake instability by powder lubrication, *Nature*, *467*,
262 doi:10.1038/nature09348.

263 Scholz, C., P. Molnar, and T. Johnson (1972), Detailed studies of frictional sliding of granite and implications for the
264 earthquake mechanism, *J. Geophys. Res.*, *77*, doi:10.1029/JB077i032p06392.

265 Scholz, C. H. (2002). The mechanics of earthquakes and faulting. Cambridge university press.

266 Scuderi, M. M., C. Marone, E. Tinti, G. Di Stefano, and C. Collettini (2016), Precursory changes in s eismic velocity
267 for the spectrum of earthquake failure modes, *Nat. Geosci.*, doi:10.1038/NGEO2775.

268 Segall, P., A. M. Rubin, A. M. Bradley, and J. R. Rice (2010), Dilatant strengthening as a mechanism for slow slip
269 events, *J. Geophys. Res.*, *115*, doi:10.1029/2010JB007449.

270 Sibson, R. H. (1977), Fault rocks and fault mechanisms, J. Geol. Soc. London, 133, 191–214.

271 Smith, S. , S. Nielsen, and G. Di Toro (2015), Strain localization and the onset of dynamic weakening in calcite fault
272 gouge, *Earth Planet. Sci. Lett.*, *413*, doi:10.1016/j.epsl.2014.12.043.

273 Tehalenko, J. S., (1970) Similarities between shear zones of different magnitudes, *Geol. Soc. Am. Bull*., 81, 1625-1640.

274 Tinti, E., M. M. Scuderi, L. Scognamiglio, G. Di Stefano, C. Marone, and C. Collettini (2016), On the evolution of
275 elastic properties during laboratory stick-slip experiments spanning the transition from slow slip to dynamic
276 rupture, *J. Geophys. Res. Solid Earth*, doi:10.1002/2016JB013545.

277 Yund, R. a., M. L. Blanpied, T. E. Tullis, and J. D. Weeks (1990), Amorphous material in high strain experimental fault
278 gouges, *J. Geophys. Res.*, *95*, 15589–15602.

Figure Caption

Figure 1. (A) Double direct shear configuration with the spring used to reduce the stiffness of the loading system. (B) Mechanical data for 6 runs at normal stresses σ_n from 13 to 35 MPa. Experiments at σ_n = 25 MPa run at higher stiffness (red and green lines) produce stable sliding. White dots represent the sampling points for microstructural studies. (C) Details of stick-slip cycles: with increasing normal stress we observe an increase in stress-drop, peak slip velocity and recurrence intervals of the cycles. Note: because the vertical LVDT is mounted on the vertical forcing block the peak slip velocity represents the average slip velocity of the entire experimental fault.

Figure 2. A and B) Fabric of faults zones recovered from experiments at σ_n = 25 MPa under high stiffness (red and green lines of Figure 1B), with stable sliding at 10 μm/s. Lower panels show enlargement of upper panels. (A) Low strain. (B) High strain. (C) Evolution of the RSF parameters with normal stress and shear strain. (D) Layer dilation during step velocity increases as a function of increasing strain. (E) Experimental fault at σ_n = 35 MPa, during stick-slips with mean-slip velocity of 3 cm/s. Localization along Y-shears contained within B shear zones. The Y-shears consist of nano-scale grains that contain intense dislocations and some fracturing (green inset). Outside the B-shear zones grains are larger and contain fractures (red inset).

Figure 3. (Upper panel) Data showing the evolution of loading stiffness k' (red dots and open circles) and rheologic stiffness, k'_c (filled black circles). Data for k' include both shear load/unload cycles and stick-slip cycles (details in Figure DR5 in GSA Data Repository). Values of k'_c are calculated from the RSF parameters (Figure 2C); grey region shows evolution of k'_c with the mean fit represented by the black line. Regions noted by 1, 2, and 3 represent the inferred evolution of microstructure as reported in the schematic at the bottom.

Figure 1

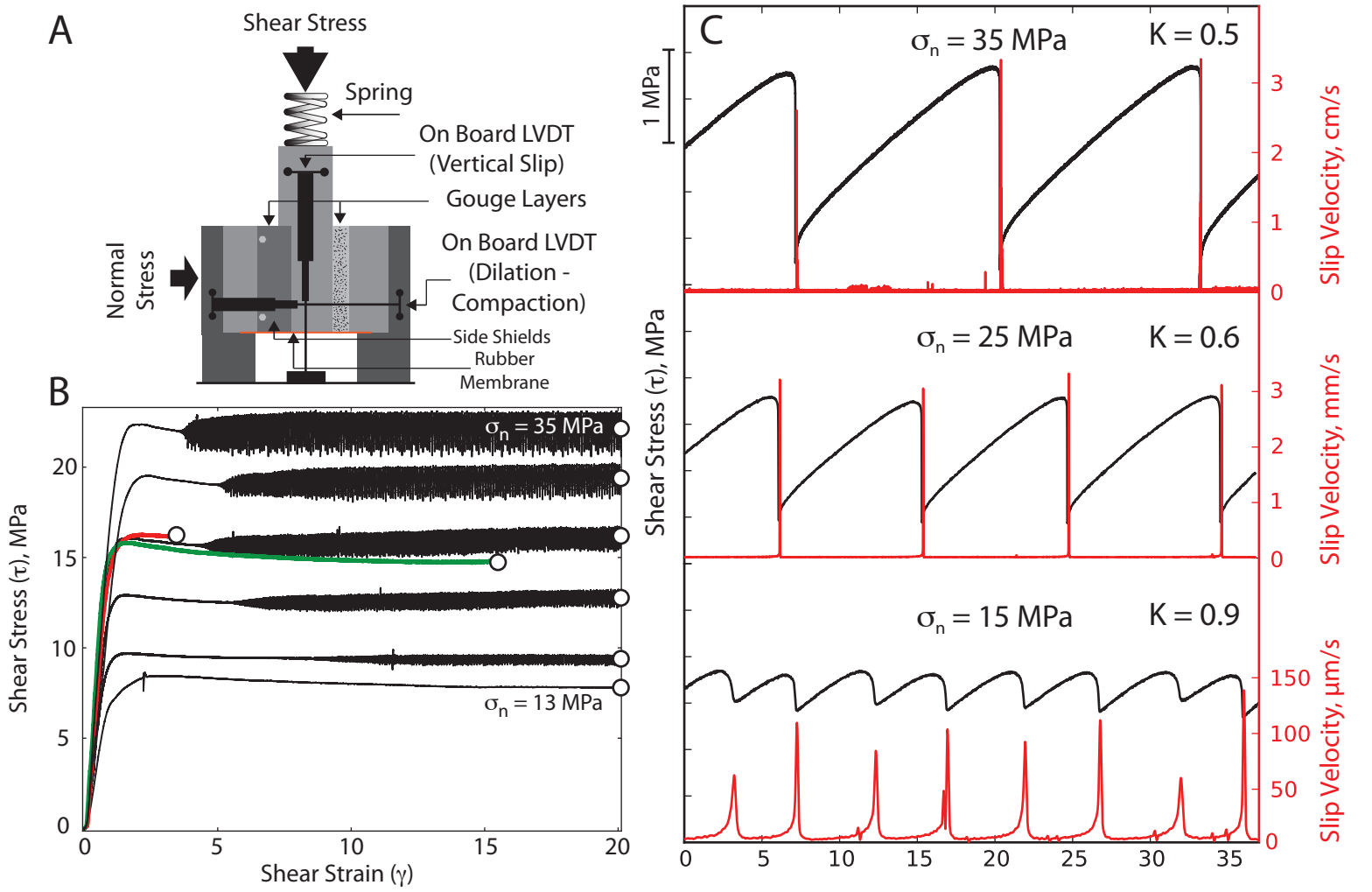

Figure 2

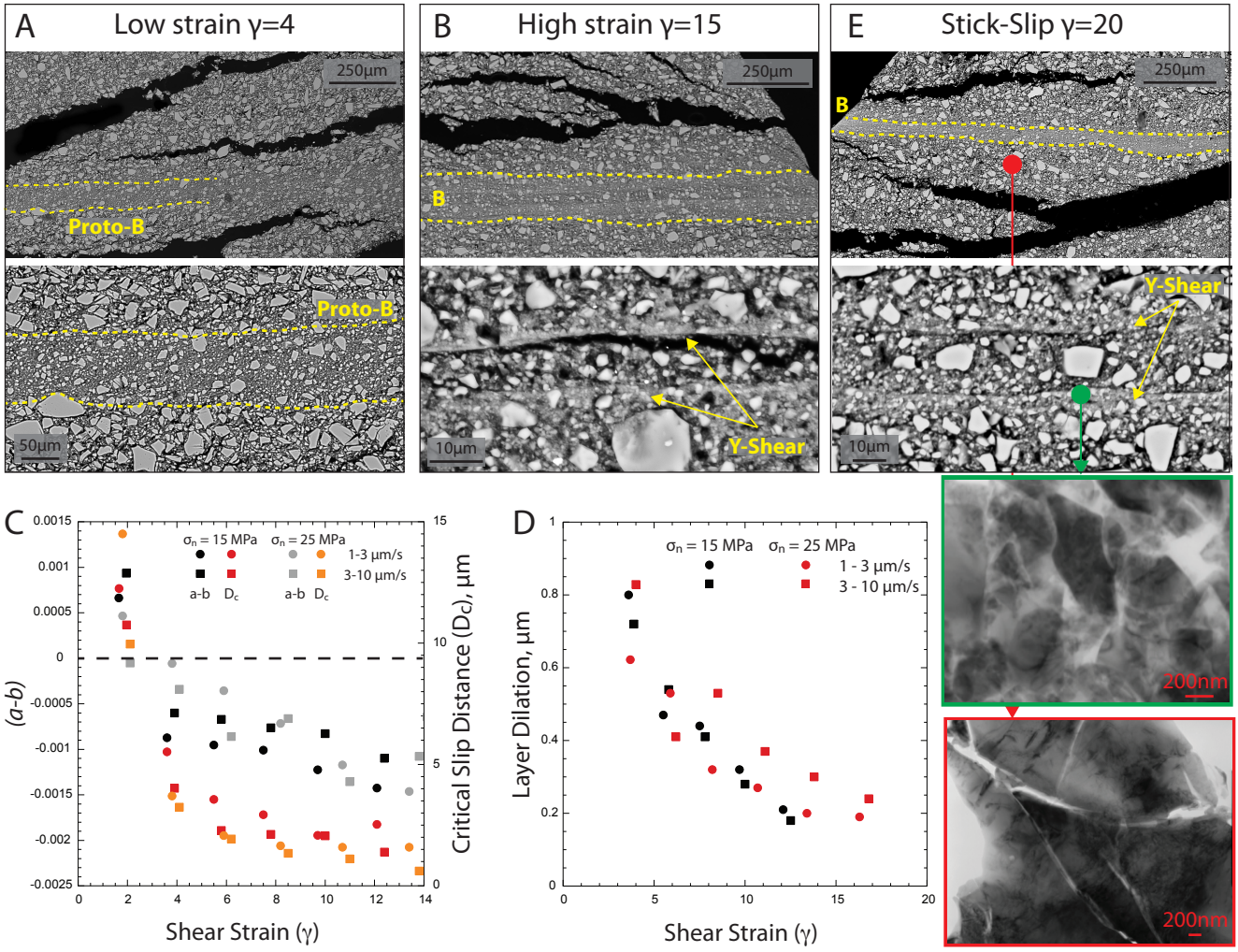

Figure 3

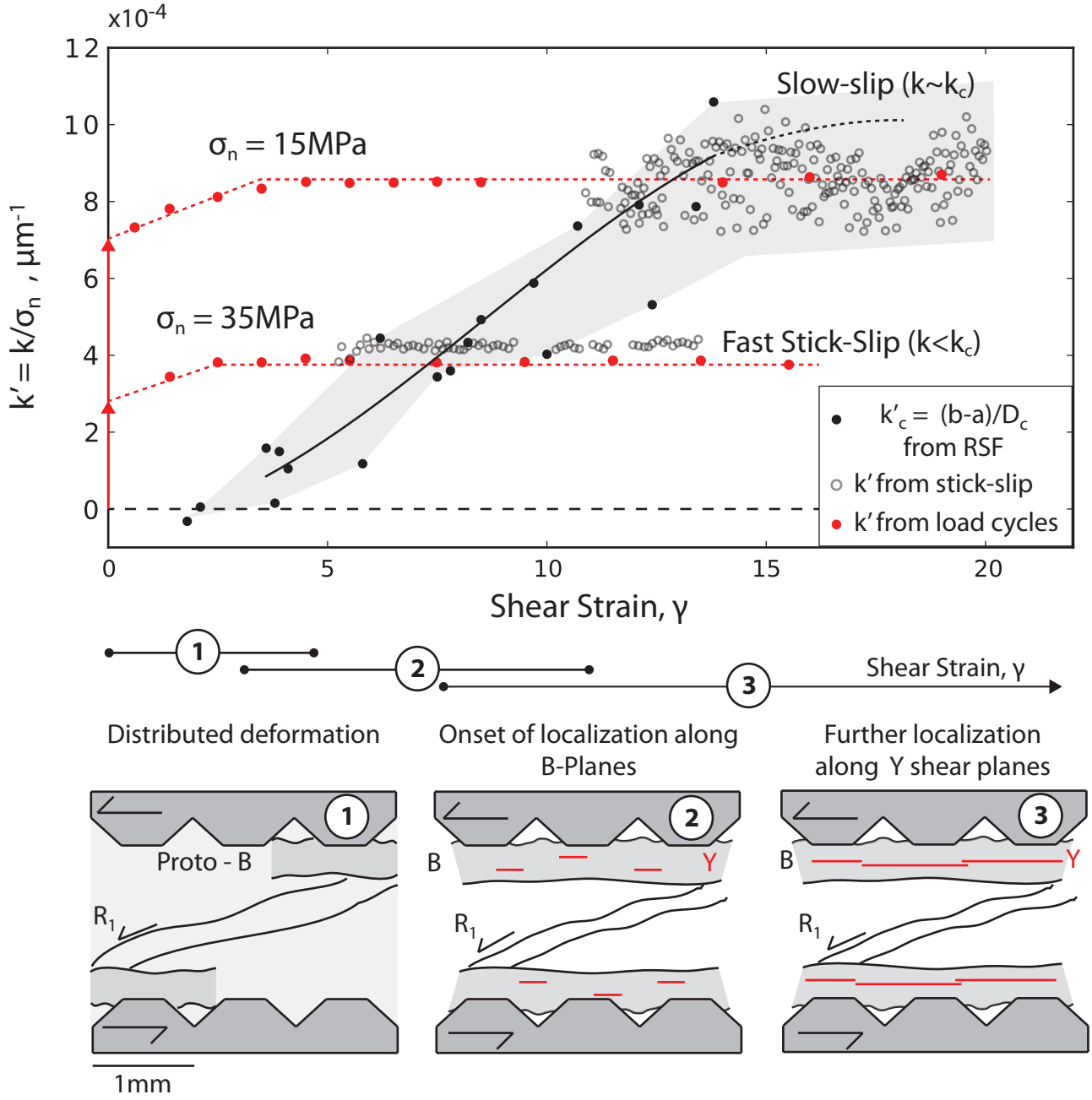

Evolution of Shear Fabric in Granular Fault Gouge From Stable Sliding to Stick-Slip and Implications for Fault Slip Mode

Authors: M.M. Scuderi[1], C. Collettini[1], C. Viti[2], E. Tinti[3] and C. Marone[4]

[1] *Dipartimento di Scienze della Terra, La Sapienza Università di Roma, Rome Italy*

[2] *Dipartimento di Scienze Fisiche, della Terra e dell'Ambiente, Università degli Studi di Siena, Siena, Italy*

[3] *Istituto Nazionale di Geofisica e Vulcanologia (INGV), Rome Italy*

[4] *Department of Geoscience, The Pennsylvania State University, University Park, PA USA*

*Correspondence to: marco.scuderi@uniroma1.it

This file includes text, figures and tables divided into seven Data Repository (DR) items:

- DR1 Summary of experiments and boundary conditions;
- DR2 Evaluation of rate and state friction parameters;
- DR3 Calculation of the dilatancy coefficient
- DR4 Details on fabric evolution from stable sliding to stick-slip;
- DR5 Characterization of the stiffness of the loading system;
- DR6 Growing of frictional instabilities for a typical experiment;
- DR7 The role of applied normal stress in the stiffness of the loading system.

DR1: Summary of experiments and boundary conditions.

Experiment number	Normal stress (MPa)	Spring	Target of the experiment	Microscopy analyses
b266	13	Yes	Stable Sliding	No
b267	14	Yes	Stick-slip	No
b268	13.5	Yes	Stable sliding	No
b371	15	Yes	Stick-slip	SEM
b372	25	Yes	Stick-slip	No
b390	15	Yes	Stick-slip	SEM
b391	25	Yes	Stick-slip	SEM/TEM
b416	15	No	Rate & State friction parameters	No
b417	25	Yes	Stick-slip	No
b417	25	Yes	Stick-slip	No
b418	20	Yes	Stick-slip	No
b418	20	Yes	Stick-slip	No
b433	25	No	Rate & State friction parameters	No
b511	25	No	Stable sliding $g = 4$	SEM
b512	25	No	Stable sliding $g = 15$	SEM
b540	30	Yes	Stick-slip	SEM
b540	30	Yes	Stick-slip	SEM
b541	35	Yes	Stick-slip	SEM
b542	15	Yes	Stick-slip	SEM
b543	35	Yes	Stick-slip	SEM
b544	35	Yes	Stick-slip	SEM/TEM
b615	35	Yes	Stiffness during loading/unloading	No
b616	15	Yes	Stiffness during loading/unloading	No
b617	35,15	Yes	Stiffness during loading/unloading	No

All tests were conducted under 100% relative humidity (RH) to ensure experimental reproducibility. All experiments were run at shear velocity of 10 μm/s, except for experiments to retrieve RSF parameter, which included velocity steps tests of 1-3-10 μm/s.

DR2: Evaluation of rate and state friction parameters

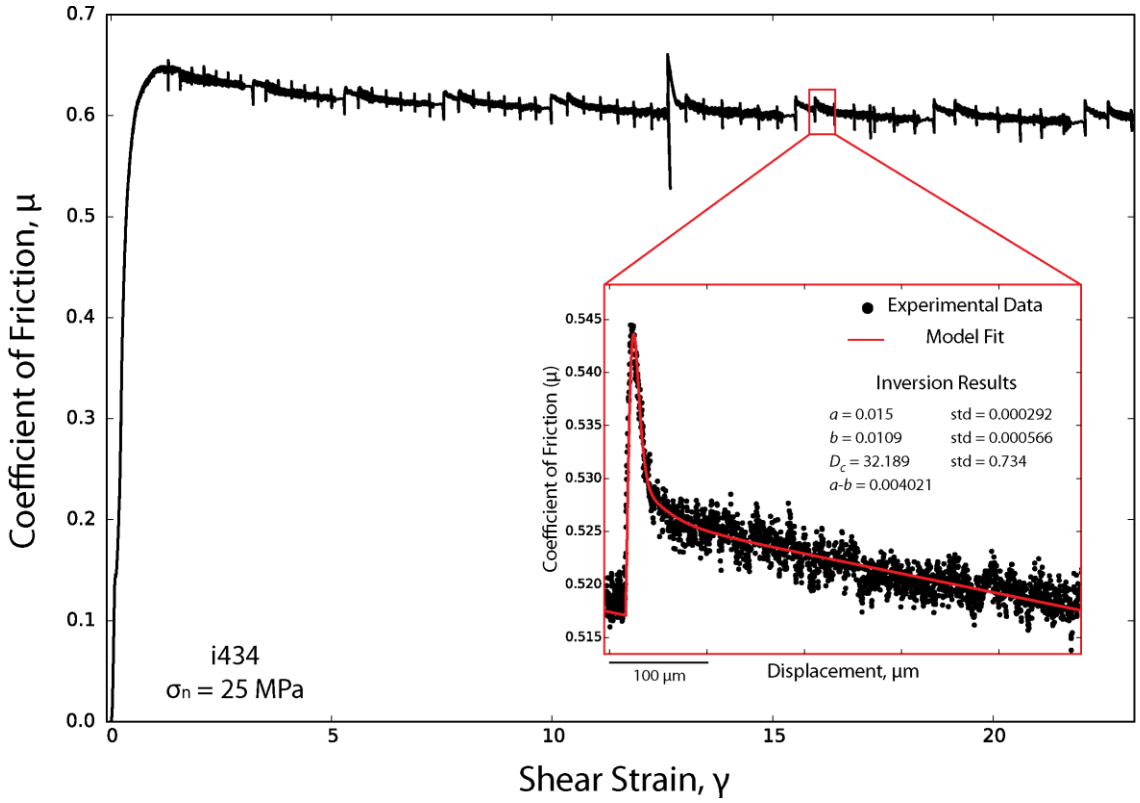

To characterize the evolution of the rate- and state- friction parameters we performed a series of velocity steps (from 1 to 10 μm/s) with increasing strain, at normal stresses of 15 and 25 MPa. To determine the rate- and state-friction parameters, *(a-b)* and D_c, we modelled each velocity step using an iterative singular value decomposition technique, which solves the rate- and state-friction equations using the Ruina evolution law coupled with the elastic interaction of the testing machine (Reinen and Weeks, 1993; Blanpied et al., 1998). The inset in red shows the details of one velocity step with the comparison between experimental data (in black) and the result from the inversion model (red).

DR3: Calculation of the dilatancy coefficient

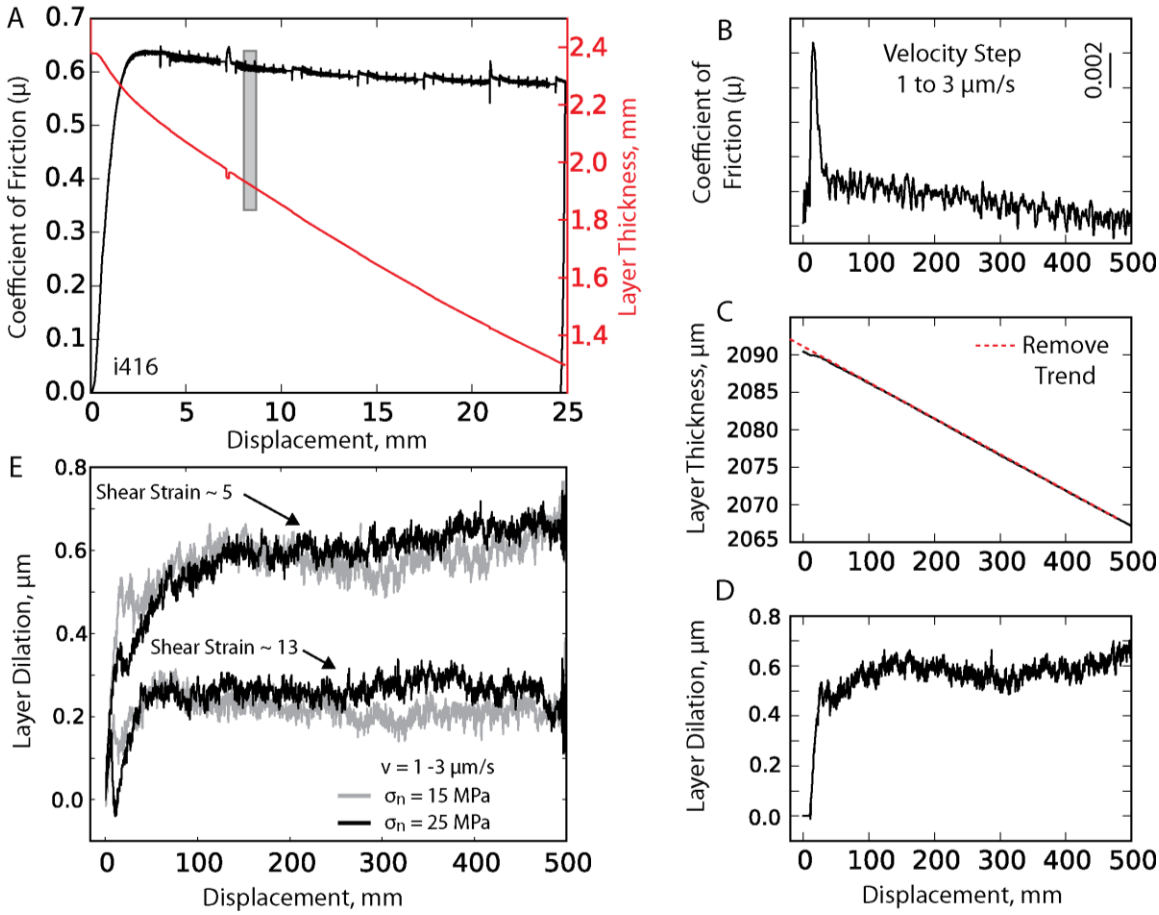

In order to investigate the degree of shear localization in response to step changes in the imposed slip velocity, we analyzed changes in gouge layer thickness measured at constant normal stress. (Panel A) Data from a typical velocity step test. Note overall geometric layer thinning with superimposed variations. Dilation associated with velocity perturbations was measured after removing geometric layer thinning due to simple shear (Scott et al., 1994). (B) Enlargement of a velocity step (grey box in Panel A), showing the evolution of frictional strength; a linear trend has been removed. (C) Raw data for layer thickness evolution during the velocity step shown in (B). Dashed red line represents the linear trend removed in order to analyze dilation, as in panel D. (D) Detrended data from Panel C showing layer dilation at higher slip velocity. (E) Comparison of layer dilation at two values of shear strain for experiments performed at 15 (grey) and 25 MPa (black) normal stress. Data have been offset so that 0,0 corresponds to the velocity step. Note that for both normal stresses the instantaneous dilation is smaller at higher strain, indicating a greater degree of shear localization

DR4: Details on fabric evolution from stable sliding to stick-slip

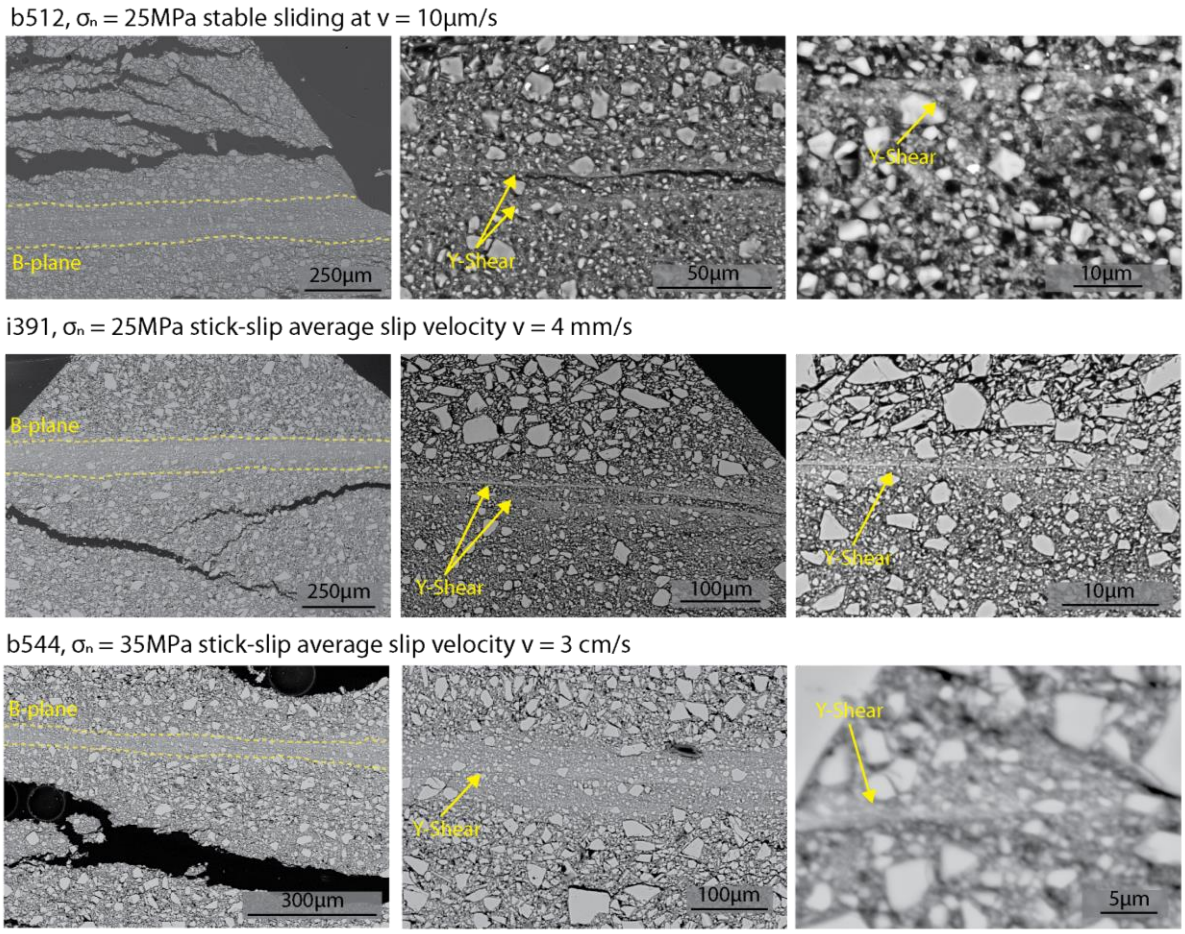

Microstructures for three layers sheared at different normal stresses and loading stiffnesses. Lower two rows are layers from dynamic, stick-slip failure. Upper row is a stable sliding experiment. Despite the different stick-slip velocities the microstructures are nearly identical. Note localization along Y-shear planes contained within B shear zones for each case. In these zones of localization the only difference between stable and unstable failure is that for higher stick-slip velocities the B shear zones show a higher level of grain-size reduction.

The images below show details of the nanostructure of Y-shear planes for different stick-slip experiments. Nano-scale structures are very similar for the two boundary conditions; each consisting of nanograins, with grain-size of < 500 nm, with intense dislocations. Nanograins likely form by dislocation pile-up during strain accumulation.

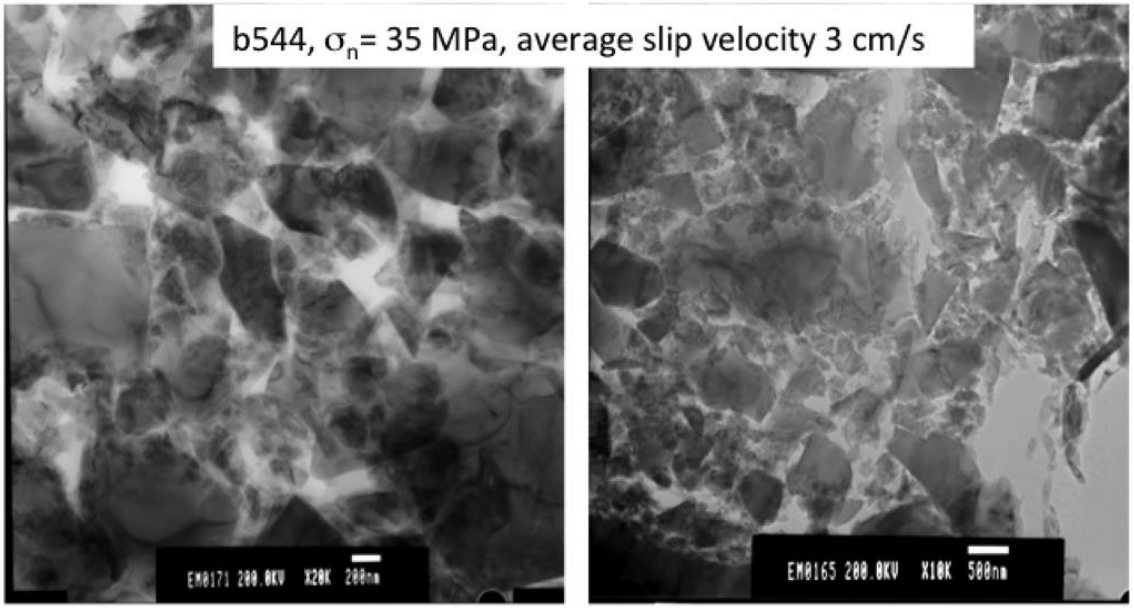
b544, σ_n= 35 MPa, average slip velocity 3 cm/s
EM0171 200.0KV X20K 200nm
EM0165 200.0KV X10K 500nm

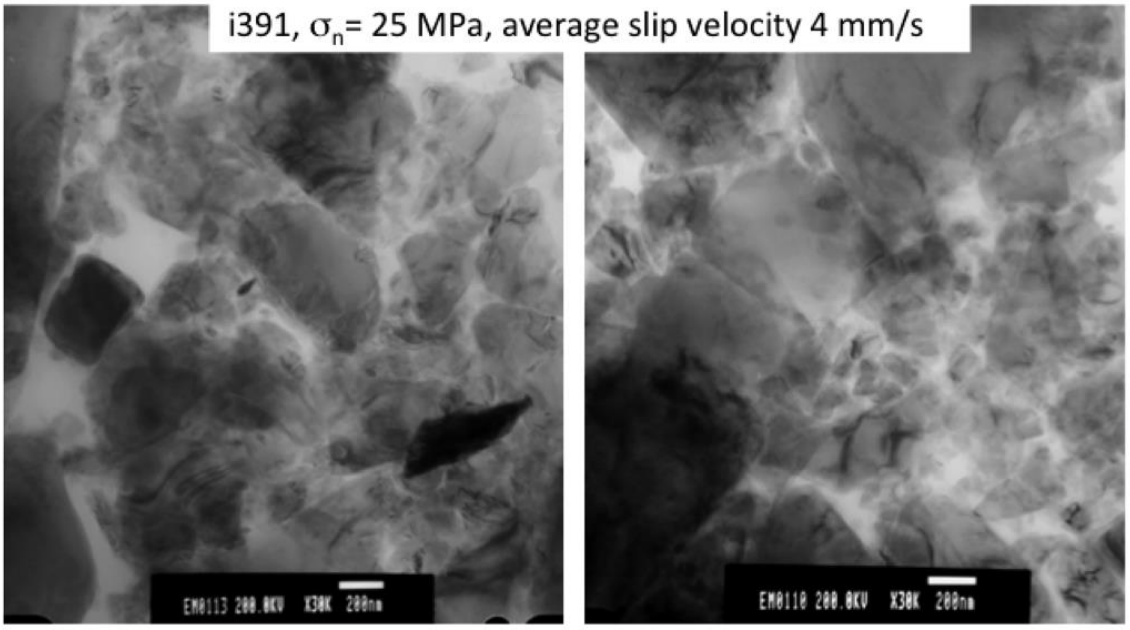
i391, σ_n= 25 MPa, average slip velocity 4 mm/s
EM0113 200.0KV X30K 200nm
EM0110 200.0KV X30K 200nm

DR5: Characterization of the stiffness of the loading system.

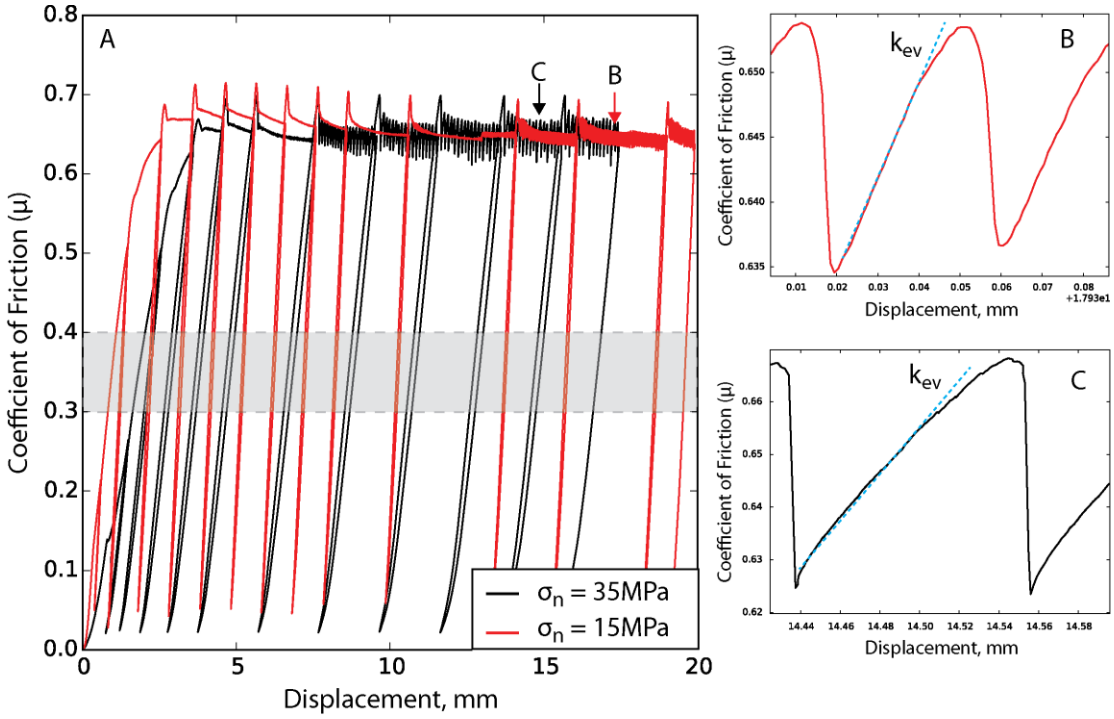

Data showing the technique used to measure loading stiffness as a function of shear stress and shear strain. The effective loading stiffness is determined by apparatus stiffness, fault gouge stiffness, and normal stress: $k' = k/\sigma'_n$. We evaluate k from load/unload cycles (panel A) and from (panels B &C) the linear, elastic sections of the stick-slip loading curves. Both methods produce similar values, indicating that the shear stress dependence of k' is minor.

DR6: Growth of frictional instabilities

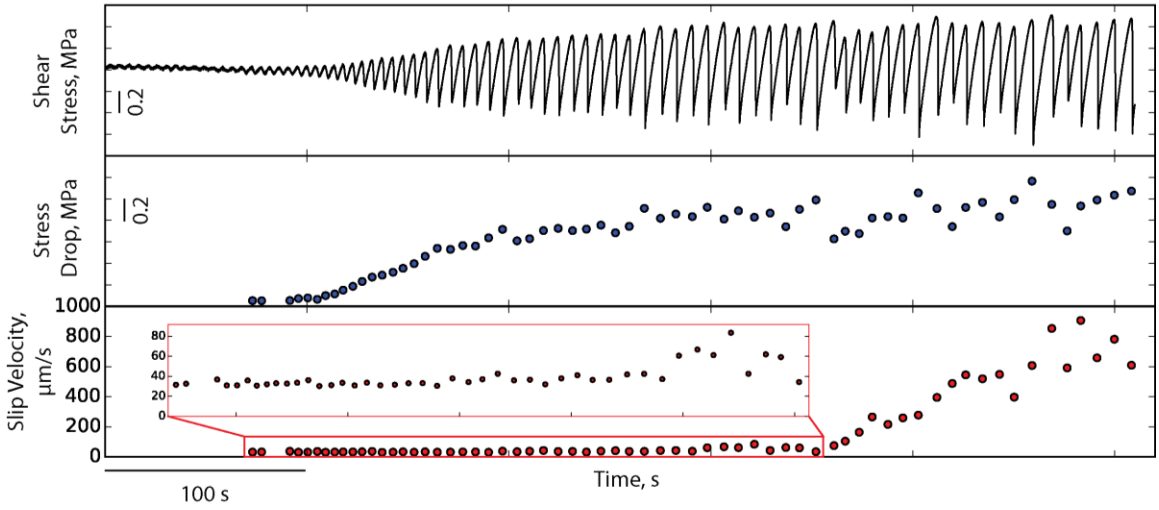

Here we show an example of the spontaneous emergence of unstable sliding with small stick-slip instabilities that initiate when K = 1, i.e. near the intersection between black and red curves (Fig. 3). With increasing displacement we observe a growing phase in stress drop and slip velocity before reaching a nearly steady state, stick-slip behaviour.

DR7: The role of applied normal stress in the stiffness of the loading system.

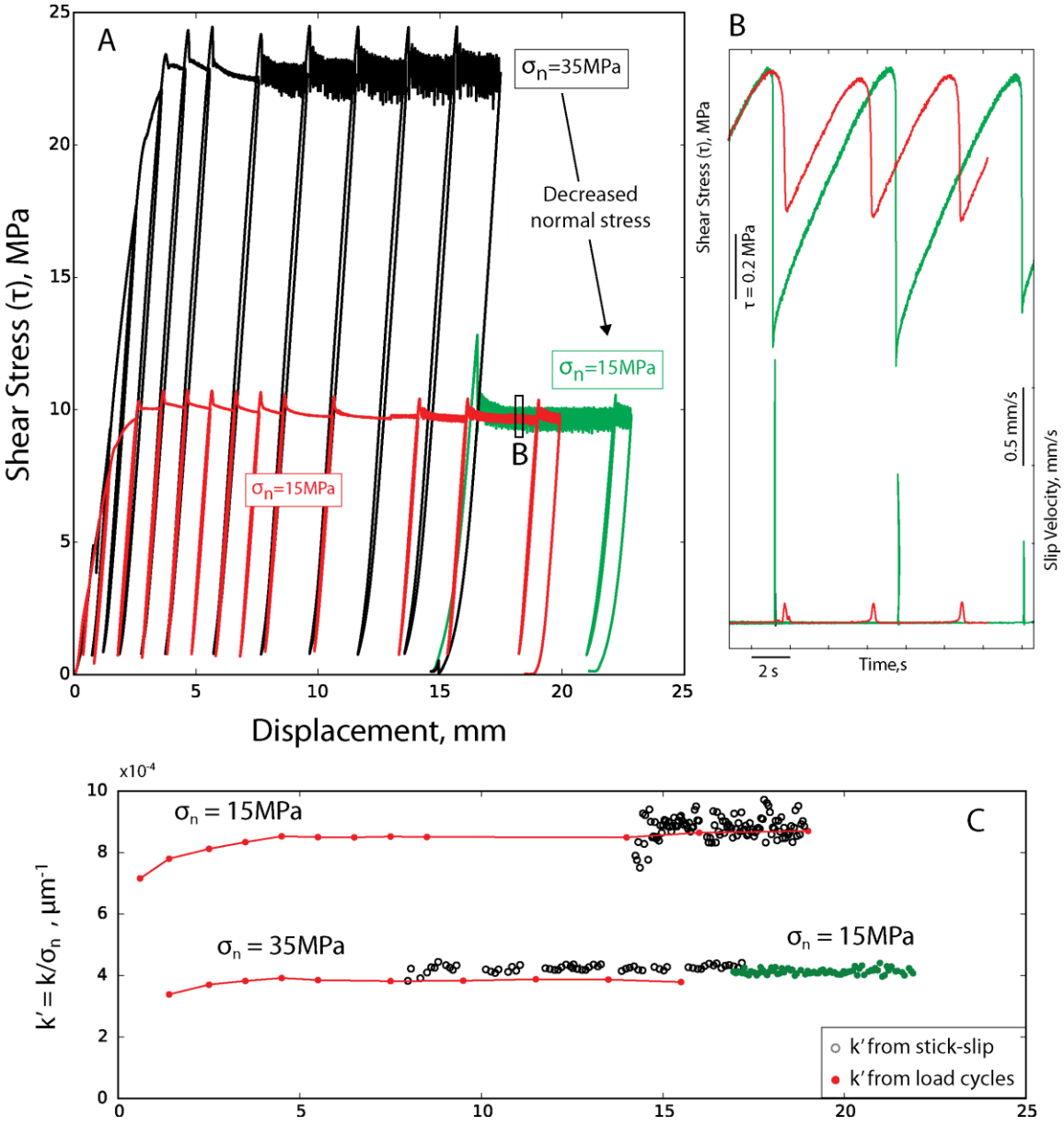

(change y axis of Panel C, as suggested for Fig 3). Elastic stiffness *k* and its evolution with shear displacement and normal stress. (A) Data for *k* at two normal stresses as determined from load/unload cycles. Red line shows data for an experiment at 15 MPa normal stress. Black and green lines show an experiment that started at 35 MPa normal stress and was reduced to 15 MPa after ~ 15 mm of shear displacement. Note that sliding is unstable for the run in which normal stress was reduced. These stick-slips are different in comparison to the "standard" stick-slips observed at 15 MPa (Figure B) because they

have shorter duration, larger stress drop (1.0 vs. 0.5 MPa), shorter rise time and faster slip velocity (1.5 vs. 0.15 mm/s). These faster stick-slip events recorded at 15 MPa result from a decrease of the stiffness of the loading system that it is acquired at 35 MPa and it is maintained when the normal stress is reduced at 15 MPa (Figure C). We interpret this increase in stiffness as a product of fabric development and fault zone stiffness. In particular the lower stiffness of the loading system is likely promoted by a more pronounced grain-size reduction favoured by higher stresses rather than stick-slip velocities, because stable values of stiffness at 35 MPa are reached after 5 mm of displacement, hence before the onset of stick-slip instabilities

References:

Blanpied, M.L.; Marone, C.J.; Lockner, D.A.; Byerlee, J.D.; King, D. P. . Quantitative measure of the variation in fault rheology due to fluid-rock interaction. *J. Geophys. Res.* **103,** 9691–9712 (1998).

Reinen, L. & Weeks, J. Determination of Rock Friction Constitutive Parameters Using an Iterative Least Squares Inversion Method. *J. Geophys. Res.* **98,** (1993).

Samuelson, J., D. Elsworth, and C. Marone (2009), Shear-induced dilatancy of fluid-saturated faults: Experiment and theory, *J. Geophys. Res.*, *114*(B12), B12404, doi:10.1029/2008JB006273.

Scott, D., C. Marone, and C. G. Sammis (1994), The apparent friction of granular fault gouge in sheared layers, *J. Geophys. Res.*, *99*, 7231–7246.